Title

Dioxygen Binding Is Controlled by the Protein Environment in Non-heme FeII and 2-Oxoglutarate Oxygenases: A Study on Histone Demethylase PHF8 and an Ethylene-Forming Enzyme.

Journal

Chemistry - A European Journal, 29(24)

Authors

Chaturvedi, Shobhit Sanjeev
Thomas, Midhun
Rifayee, Simahudeen
et al.

Publication Date

2023-04-25

DOI

10.1002/chem.202300138

Peer reviewed

HHS Public Access

Author manuscript

Chemistry. Author manuscript; available in PMC 2024 April 25.

Published in final edited form as:

Chemistry. 2023 April 25; 29(24): e202300138. doi:10.1002/chem.202300138.

Dioxygen Binding is Controlled by the Protein Environment in Non-Heme Fe(II) and 2-Oxoglutarate Oxygenases – A Study on Histone Demethylase PHF8 and an Ethylene Forming Enzyme

Shobhit S. Chaturvedi[a,+], **Midhun George Thomas**[a,+], **Bathir JSR Simahudeen**[a], **Walter White**[a], **Jon Wildey**[b], **Cait Warner**[c], **Christopher J. Schofield**[d], **Jian Hu**[e,f], **Robert P. Hausinger**[e,g], **Tatayana G. Karabencheva-Christova**[a], **Christo Z. Christov**[a]

[a]Department of Chemistry, Michigan Technological University, Houghton, MI 49931, USA.

[b]Department of Chemical Engineering, Michigan Technological University, Houghton, MI 49931, USA.

[c]Department of Biology, Michigan Technological University, Houghton, MI 49931, USA.

[d]The Chemistry Research Laboratory, Department of Chemistry and the Ineos Oxford Institute for Antimicrobial Research, University of Oxford, Mansfield Road, OX1 3TA, United Kingdom.

[e]Department of Biochemistry and Molecular Biology, Michigan State University, East Lansing, MI 48824, USA.

[f]Department of Chemistry, Michigan State University, East Lansing, MI 48824, USA.

[g]Department of Microbiology and Molecular Genetics, Michigan State University, East Lansing, MI 48824, USA.

Abstract

This study investigates dioxygen binding and 2-oxoglutarate (2OG) coordination by two model non-heme Fe(II)/2OG enzymes: a class 7 histone demethylase (PHF8) that catalyzes the hydroxylation of its H3K9me2 histone substrate leading to demethylation reactivity and the ethylene-forming enzyme (EFE) that catalyzes two competing reactions of ethylene generation and substrate L-Arg hydroxylation. Although both enzymes initially bind 2OG using an *off-line* 2OG coordination mode, in PHF8, the substrate oxidation requires a transition to an *in-line* mode, whereas EFE is catalytically productive for ethylene production from 2OG via the *off-line* mode. We utilized classical molecular dynamics, quantum mechanics/molecular mechanics (QM/MM) MD and QM/MM metadynamics simulations to reveal that it is the dioxygen binding process and, ultimately, the protein environment that control the formation of the *in-line* Fe(III)-$OO^{-\cdot}$ intermediate in PHF8 and the *off-line* Fe(III)-$OO^{-\cdot}$ intermediate in EFE.

Graphical Abstract

Corresponding Author: Christo Z. Christov: christov@mtu.edu, https://chem.sites.mtu.edu/christov/.

[+]These authors contributed equally to this work.

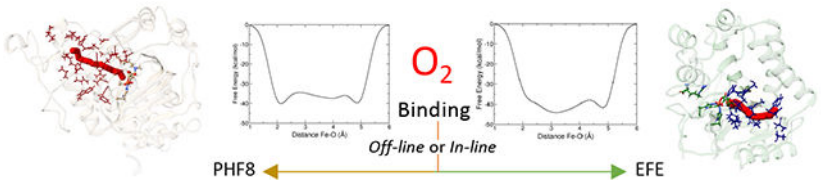

Study on the dioxygen binding and 2OG coordination by two model 2OG enzymes: a class 7 histone demethylase (PHF8) and the ethylene-forming enzyme (EFE).

Keywords

dioxygen diffusion; ethylene forming enzymes; histone demethylation; molecular dynamics; QM/MM metadynamics

Introduction

Non-heme Fe(II) and 2-oxoglutarate (2OG) dependent oxygenases catalyze a wide variety of reactions such as hydroxylation, halogenation, desaturation, epoxidation, demethylation, endoperoxidation, and ethylene generation.[1,2] Most of these diverse reactivities utilize a well-established mechanism of dioxygen binding to the five-coordinate non-heme Fe(II)-center leading to the formation of a Fe(III)-$OO^{-\cdot}$ intermediate, followed by an attack on the 2OG, and oxidative decarboxylation to form succinate and an Fe(IV)=O (ferryl) species.[3–6] The ferryl intermediate then performs the diverse reactions mentioned above, as demonstrated by computational and experimental studies.[1,7] However, in the case of the 2OG dependent ethylene-forming enzyme (EFE), recent experimental evidence has indicated its unique ethylene producing mechanism diverges during the reaction of the dioxygen with 2OG before the formation of a ferryl intermediate.[8–11] Ethylene production by EFE requires the binding of L-arginine (L-Arg), and the enzyme also catalyzes a separate, more typical reaction in which L-Arg is hydroxylated at C5 leading to the elimination of guanidine and formation of L-Δ^1-pyrroline-5-carboxylate (P5C).[8–10] The role of the L-Arg substrate orientation in the EFE catalysis has been studied experimentally[9,10] and computationally[12,13]. These results indicate that 2OG dependent oxygenases may utilize the Fe(III)-$OO^{-\cdot}$ intermediate for multiple reaction outcomes.

Crystal structures of 2OG enzymes show that 2OG can coordinate to the non-heme Fe(II)-center either in an *off-line* or an *in-line* binding mode (Figure S1).[14–18] Both 2OG binding modes utilize the C1 carboxylate and C2 keto of 2OG to ligate the Fe(II)-center in the same plane with a His residue and an Asp/Glu residue, with axial coordination by another His residue. For the *in-line* binding mode, the often open (aside from sometimes a water is present) sixth coordination position is proximal to the substrate.[14,18] Dioxygen binding to such an arrangement is expected to generate an *in-line* Fe(III)-$OO^{-\cdot}$ intermediate.[19] For the *off-line* binding mode of 2OG, the vacant sixth coordination position is not adjacent to the substrate and causes *off-line* Fe(III)-OO^{-}.[14,18,19] The roles of *off-line* and hypothetical *in-line* Fe(III)-$OO^{-\cdot}$ intermediates in influencing the reactivity are demonstrated in a computational study of EFE.[12] That study predicted the transformation of a five-coordinated (5C) *off-line* ES complex to *in-line* is energetically unfavorable with an energy

barrier of 21.8 kcal/mol and the formed 5C *in-line* ES complex is highly endothermic by 20.9 kcal/mol[12] thus being in agreement with the experimental[8,20] and computational data[11] that the *off-line* binding mode is the one that persists in the subsequently formed Fe(III)-$OO^{-\cdot}$ Intermediate. We furthermore demonstrated a hypothetical *in-line* Fe(III)-$OO^{-\cdot}$ intermediate would exclusively lead to L-Arg hydroxylation in EFE while the *off-line* Fe(III)-$OO^{-\cdot}$ intermediate generates both ethylene and the hydroxylated substrate.[12] Computational studies on histone lysine demethylase (PHF8) and the DNA demethylases AlkB and AlkBH2, which first hydroxylate the substrate in their demethylation mechanisms, have suggested that these non-heme Fe(II) and 2OG dependent enzymes form an *in-line* Fe(III)-$OO^{-\cdot}$ intermediate in an energetically favorable step for efficient catalysis despite the presence of an initially *off-line* bound 2OG.[19,21] Mechanistic pathways for PHF8 and EFE enzymes are shown in Schemes S1 and S2 respectively. Although the reaction mechanisms of dioxygen activation and substrate oxidation in Fe(II)/2OG enzymes have been intensively studied,[1,4,22–25] the processes of dioxygen transport and binding are much less studied[26,27], especially in the context of delineating the factors that might control *in-line* versus *off-line* dioxygen binding.

The second coordination sphere (SCS) and protein environment in general are largely involved in enzyme catalysis.[25,28–32] The focus of this study is to explore the *specific interactions* in the SCS and beyond that control the dioxygen transport and binding in two Fe(II)/2OG enzymes – PHF8 that utilizes *in-line* mode and EFE that implements exclusively *off-line* mode. Here, we use computational methods to investigate whether the dioxygen binding and interactions with SCS residues in Fe(II)/2OG oxygenases to determine the formation of either an *in-line* or *off-line* Fe(III)-$OO^{-\cdot}$ Intermediate, which further influences their reaction mechanisms. To probe this hypothesis, we selected two models of non-heme Fe(II) and 2OG-dependent oxygenases from different structural subfamilies: (i) PHF8 that performs a canonical N-methyl-group hydroxylation of the histone 3 (H3) substrate during its demethylation mechanism, which is coupled with the oxidation of 2OG to succinate and CO_2 and (ii) EFE that catalyzes an alternate type of reactivity – forming ethylene directly from 2OG, along with the more typical 2OG oxidation coupled hydroxylation of substrate L-Arg. We performed quantum mechanics/molecular mechanics (QM/MM), molecular dynamics (MD) calculations on the enzyme substrate (ES) complex of PHF8 and EFE, dioxygen diffusion simulations, and further explored dioxygen binding to the non-heme Fe(II)-center using QM/MM metadynamics (QM/MM MetD) simulations.

Results and Discussions

Flexibility of the Five-Coordinated (5C) Fe(II)-Center in the Enzyme Substrate Complexes of PHF8 and EFE

Previous QM/MM potential energy calculations have explored the 2OG binding mode preferences for PHF8 and EFE.[12,19] The QM/MM calculations on PHF8 indicated that the conversion from *off-line* to *in-line* binding mode involves a low activation energy of 1.48 kcal/mol and occurs at the 5-coordinate ES state, with both 2OG and protein substrate bound, but before the dioxygen activation step.[19] By contrast, QM/MM calculations on EFE have indicated a clear preference for the *off-line* binding mode of 2OG in the ES

complex (with both 2OG and L-Arg bound), with an activation energy required for the rearrangement from *off-line* to *in-line* coordination mode of 21.8 kcal/mol.[12] In this study, we first explored if 2OG retains the *off-line* binding mode or if it changes spontaneously from an *off-line* to an *in-line* mode during the time-dependent fluctuations of the Fe(II)-center in the two enzymes using unbiased QM/MM MD simulations. The QM/MM MD simulations showed that the average dihedral angle for N_{H247}-Fe-O2-O1 (Figure S2A) for PHF8 was 111° and N_{H189}-Fe-O2-O1 (Figure S2B) for EFE was 116°. During the simulation, the dihedral angle varied between 82–144° for PHF8 and 77–159° for EFE (Figures S3 and S4). The increased flexibility of the 2OG is expected due to the open coordination state. For both systems, the dihedral angle did not reach the value seen in the QM/MM *in-line* binding of 2OG (149° for PHF8 and 168° for EFE).[12,19] These results indicate that although the simulations reveal the non-heme Fe(II)-centers in both enzymes are internally flexible, the 2OG does not undergo spontaneous rearrangement from an *off-line* binding mode to an *in-line* binding mode. We, therefore, tested whether the binding of dioxygen could be the key factor for such a transition. For this aim, we performed dioxygen diffusion and binding calculations on both systems.

Dioxygen diffusion in PHF8

The MD simulations of the dioxygen diffusion dynamics in PHF8 explored two potential dioxygen transport tunnels. Analysis of the tunnels shows that the most probable tunnel for oxygen diffusion is tunnel-1. This primary oxygen diffusion tunnel in PHF8 is formed by a combination of residues belonging to the substrate histone peptide and all three regions of PHF8, that is, the plant homeobox (PHD) domain, the linker, and the catalytic JmjC domain (Figure 1A). The characteristics of the oxygen transport tunnels were analyzed using CAVER 3.0.[33] Tunnel-1 is 23.7 Å long and has a bottleneck radius of 0.9 Å. The tunnel-1 entry gate has a radius of about 2.2 Å and is surrounded by predominantly charged or hydrophilic residues - E39, E40, K41, K81, R164, Q165, D167, N289, E290 - with a few more hydrophobic residues, including A43 and A166 (Figure S5). During transport from the exterior of PHF8 to the active site via tunnel-1, the dioxygen molecules interact with hydrophobic residues such as I160, F246, and W282, apparently making hydrogen bond with D245, Q288, and N289 of PHF8, and interacting with substrate's H3A7 and H3R8 (Figure S6). The dioxygen molecules moving through tunnel-1 approach the Fe(II)-center for binding in a direction *trans* to H319. Such an approach of dioxygen would require a rearrangement of 2OG to allow binding to the Fe(II)-center, forming an *in-line* Fe(III)-$OO^{-\cdot}$ complex (Figure 1B). This dioxygen approach is facilitated by the hydrophobic interactions with the side chains of the H3K9me2 substrate and the enzyme residues I191 and T244 (Figures 1B and S7).

After reaching the Fe(II)-center through tunnel-1 a few dioxygen molecules were observed to 'cross over' the C3-C5 carbon chain of 2OG by interacting with the residues N189, V190, I191, S192, L236, S238, T244, and K264 (Figure S8). After the crossover, a dioxygen molecule approaches the Fe(II)-center in *trans* position to H247 and is stabilized by the hydrophobic residues V255, Y257, F266, L311, and I313 (Figure S9). The Fe(III)-$OO^{-\cdot}$ complex formed upon dioxygen binding from this direction is an *off-line* Fe(III)-$OO^{-\cdot}$ complex (Figure 1C).

Tunnel-2 also leads to an approach of the dioxygen molecules *trans* to H247 and results in the formation of an *off-line* Fe(III)-$OO^{-\cdot}$ complex, as described in the SI (Pages 7–8). *Thus, the MD simulation reveals two tunnels used by dioxygen molecules to diffuse from the surface to the active site of PHF8, and it demonstrates that dioxygen can approach the Fe(II)-center for binding from two directions* – trans *to H247 (Off-line approach) and/or* trans *to H319 (In-line approach)*.

Dioxygen diffusion in EFE

The dioxygen diffusion dynamics in EFE also indicate two likely transport channels. The primary diffusion tunnel in EFE (tunnel-1) is shorter than the PHF8 dioxygen diffusion tunnel-1 with a total length of 18.9 Å and a bottleneck radius of 1.15 Å (Figure 2A). Apparent gatekeeper residues for tunnel-1 entry in EFE are Q200, D202, T243, V246 (Figure S10). While diffusing through EFE tunnel-1, the dioxygen molecules interact with A198, A199, L206, W247, T248, R277, A279, C280 (Figure S11). The approach of the dioxygen from tunnel-1 is *trans* to H189 and can lead to a formation of an *off-line* Fe(III)-$OO^{-\cdot}$ complex without 2OG rearrangement (Figure 2B). At the active site, the dioxygen molecule is stabilized for binding to the Fe by interactions with hydrophobic residues V196, F250, A281, and F283 (Figures 2B and S12).

An alternative to EFE tunnel-1, tunnel-2 is described in the SI (Page 8), which enables the approach of the dioxygen *trans* to H268 and which therefore is positioned to form an *in-line* Fe(III)-$OO^{-\cdot}$ complex (Figure 2C). *Thus, the MD study of the EFE dioxygen diffusion revealed two tunnels used by the dioxygen molecules to diffuse from the surface to the active site of EFE. Like the results in PHF8, dioxygen diffusion dynamics in EFE indicate that dioxygen can approach the Fe-center for binding from two directions – either* trans *to H189 and/or* trans *to H268*.

The calculations of dioxygen diffusion demonstrated that in both enzymes, the protein tunnels might deliver the dioxygen to positions for either *off-line* or *in-line* binding to the Fe(II) center. To explore the chemical mechanism of dioxygen binding, we performed QM/MM MetD simulation at the septate spin surface as we demonstrated that the crossing to the quintet spin state happens at the product state (Figure S13). Additional details about the different spin state surfaces of the dioxygen binding to Fe(II) are provided in the SI (Pages 14–15).

Dioxygen binding to the Fe(II)-center in PHF8

We then performed QM/MM–MetD simulations to explore which of the two dioxygen binding possibilities in PHF8 proceeds with a lower activation free energy and leads to an energetically favorable and stable Fe(III)-$OO^{-\cdot}$ complex.

In-line dioxygen binding

The septet spin state QM/MM-MetD simulation for *in-line* binding of a dioxygen molecule indicates the reactant complex (RC) conformations, corresponding to an Fe-O distance of 4.8 Å (Figure 3). The analysis of a representative RC structure from the QM/MM MetD simulation (Figure 3C) shows that the N_{H247}-Fe-O2-O1 dihedral angle is 93.1°, indicating

that the 2OG maintains an *off-line* binding mode. The bond length of the Fe(II) and C1 carboxylate oxygen (Fe-O1) bond is 2.1 Å and the Fe and C2 keto oxygen (Fe-O2) bond length is 2.3 Å compared to average values of 2.1 Å and 2.2 Å in previous QM/MM optimized PHF8 ES complexes.[34] H247, D249, and H319 coordinate the Fe(II)-center, with monodentate coordination of D249 and the dioxygen, approaches the Fe(II)-center for binding *trans* to H319. The free energy required to cross the *in-line* dioxygen binding transition state (TS) starting from the unbound RC conformations of dioxygen and the Fe(II)-center is 6.0 kcal/mol (Figure 3A). A representative structure of the TS (Figure 3D) shows an Fe-O distance of 2.7 Å, and Fe-O1 and Fe-O2 bond lengths are maintained at 1.9 Å and 2.2 Å. However, the N_{H247}-Fe-O2-O1 dihedral angle changes to 143.1°, indicating a transition of 2OG from the *off-line* binding mode towards *in-line* binding. *The geometric analysis indicates that hydrophobic interactions with the H3K9me2 sidechains, I191 and T244, orient and stabilize the dioxygen molecule binding to Fe(II) at the TS structure* (Figure 3D). The reaction completes with the formation of an *in-line* bound Fe(III)-$OO^{\cdot-}$ complex that is 0.8 kcal/mol higher in energy compared to the unbound dioxygen and Fe(II) complex (Figure 3A). A representative structure of the product complex (PD) (Figure 3E) with an Fe-O distance of 2.1 Å shows that the dioxygen is bound in an end-on fashion to the Fe(II)-center at a position *trans* to H319. As the dioxygen binds to the Fe-center, the 2OG rearranges completely to an *in-line* binding mode with a N_{H247}-Fe-O2-O1 dihedral angle of 174.1°. The 2OG maintains its bidentate mode with the Fe-C1 carboxylate oxygen bond length of 1.9 Å and the Fe-C2 keto oxygen with a slightly elongated bond length of 2.4 Å. The optimized structure of the product confirms the *in-line* coordination mode of the dioxygen and 2OG. *The results on 2OG binding mode in PHF8 are in agreement with the PHF8 crystal structures where 2OG is found to coordinate to the Fe(II) in an in-line fashion without the H3 substrate but changes to an off-line coordinate mode when the H3 substrate is bound.*[35,36]

Off-line dioxygen binding

The QM/MM-MetD simulation shows that the RC for *off-line* binding of the dioxygen molecule to the Fe(II)-center is characterized by the same Fe-O distance of 4.8 Å as in the *in-line* RC. The N_{H247}-Fe-O2-O1 dihedral angle shows that the 2OG maintains an *off-line* binding mode, though with a slightly greater dihedral angle of 118° compared to 93° for the *in-line* dioxygen binding RC. The Fe-O1 and Fe-O2 bond lengths are 2.1 and 2.3 Å, respectively. Similar to the *in-line* dioxygen binding RC, the H247, D249, and H319 ligands maintain monodentate coordination to the Fe(II)-center. However, a sixth open coordination site in the *off-line* dioxygen binding RC is available *trans* to H247. Interactions with Y234, V255, Y257, F266 and I313 stabilize the dioxygen molecule for *off-line* binding in the active site (Figure S14). These interactions are different from the interactions that stabilize *in-line* dioxygen binding. The free energy surface on the septet spin state shows that the dioxygen approach for binding to the Fe(II)-center from the position *trans* to H247 requires an activation energy of 27 kcal/mol and does not seem to form a stable *off-line* bound Fe(III)-$OO^{\cdot-}$ complex (Figure 3B). To test if the spin state might be a reason for the instability of the Fe(III)-superoxo intermediate, we repeated the QM/MM-MetD simulation for both the *in-line* and *off-line* binding of the dioxygen at the quintet spin state (Figures S15 and S16). Calculations indicated that the free-energy barrier required to cross the quintet

off-line dioxygen binding transition state is similarly high at 22.8 kcal/mol and the *off-line* dioxygen bound Fe(III)-$OO^{\cdot -}$ product is endothermic by 21.0 kcal/mol in comparison to the RC (unbound Fe(II) and dioxygen) (Figure S16).

Analysis of both the septet and quintet spin state trajectories shows that for the *off-line* approach to the Fe(II)-center, in the structures close to the TS, the dioxygen molecule has an unfavorable steric interaction with the non-coordinating carboxylate oxygen atom of the Fe-coordinating D249 (Figure S16). However, this interaction is minimized as the non-coordinating carboxylate oxygen atom of D249 moves away from the dioxygen by changing the C_α-C_β-C_γ-C_δ dihedral angle of D249. The strain on the sidechain is released by switching the coordinating oxygen atom of D249 from OD1 to OD2 (Figure S17). A notable observation is that during the change in coordination of the D249 oxygen, 2OG rearranges from *off-line* coordination to an *in-line* coordination mode. Therefore, the high activation energy requirement for dioxygen binding in the *off-line* binding mode in PHF8 might be partly due to the high energy required to overcome the repulsion between the dioxygen molecule and the non-coordinating oxygen atom of D249.

Thus the results of dioxygen binding in PHF8 indicate that the formation of an in-line Fe(III)-$OO^{-\cdot}$ in PHF8 is energetically favorable compared to an off-line Fe(III)-$OO^{-\cdot}$ intermediate. Supporting this assignment, QM/MM minimization of the *in-line* product from the QM/MM metadynamics simulation led to a stable, optimized structure, whereas no stable minimum energy structure was obtained after the QM/MM optimization of the *off-line* product from QM/MM metadynamics simulations. *Furthermore, the 2OG is predicted to undergo a rearrangement in binding from off-line to in-line during the dioxygen binding in PHF8*.

Dioxygen binding to the Fe-center in EFE

Similar to the situation for PHF8, we performed QM/MM MetD simulations for dioxygen binding to EFE to explore the free energy surfaces of the reactions that lead to *in-line* Fe(III)-$OO^{-\cdot}$ or *off-line* Fe(III)-$OO^{-\cdot}$.

In-line dioxygen binding in EFE

The QM/MM-MetD simulation for *in-line* dioxygen binding to EFE shows an Fe-O distance of 4.8 Å in the RC (Figure 4A). The N_{H189}-Fe-O2-O1 dihedral angle in a representative RC structure exhibited a dihedral angle of 105° (Figure S18). The Fe-O1 bond length is 2.1 Å while the Fe-O2 bond is elongated to 2.8 Å. The free energy surface on the septet spin state indicates that the dioxygen approach for binding to the Fe(II)-center occurs *trans* to H189 and proceeds with an activation energy of 8.1 kcal/mol; however, the calculation indicates that the resulting *in-line* bound Fe(III)-$OO^{\cdot -}$ complex is not energetically stable (Figure 4A). Further analysis of the trajectory indicates that as a dioxygen molecule approaches the Fe(II)-center for *in-line* binding, the 2OG changes to monodentate coordination with Fe(II) (Figure S17). The observed unusual monodentate coordination mode of 2OG is similar to an observed monodentate 2OG coordination in EFE crystal structures lacking the L-Arg substrate(Figure S19).[9] Comparable switching of 2OG from bidentate to monodentate during dioxygen diffusion was observed in PHD2.[27] Thus, the results indicate that as

dioxygen approaches for *in-line* binding to EFE, there is a rearrangement to an unusual monodentate coordination mode of 2OG that is not energetically favorable for the formation of a stable *in-line* bound Fe(III)-$OO^{\cdot-}$ complex.

Off-line dioxygen binding in EFE

The septet spin state QM/MM MetD simulation for *off-line* binding of dioxygen to EFE shows Fe-O distance of 4.8 Å in the RC (Figures 4B and 4C), 2OG maintains a bidentate coordination with Fe, and the Fe-O1 and Fe-O2 bond lengths are 2.0 and 2.4 Å, respectively, compared to the 2.1 and 2.8 Å distances for the *in-line* dioxygen binding RC (Figure 4A). The N_{H189}-Fe-O2-O1 dihedral angle is 120°, indicating that 2OG maintains an *off-line* binding mode. The open coordination site for dioxygen binding is available *trans* to H189. The free energy required to cross the *off-line* dioxygen binding transition state is 3.8 kcal/mol compared to 8.1 kcal/mol for the *in-line* dioxygen binding (Figure 4). A representative TS structure (Figure 4D) shows an Fe-O distance of 4.4 Å, with the Fe-O1 and Fe-O2 bond lengths maintained at 1.9 Å and 2.6 Å. The N_{H189}-Fe-O2-O1 dihedral angle of 2OG is slightly greater at 127°, compared to the EFE *in-line* dioxygen binding TS. *The hydrophobic interactions with A198, F250, A281, and F283 stabilize off-line dioxygen binding to Fe at the TS* (Figure 4). The reaction completes with the formation of an *off-line* bound Fe(III)-$OO^{\cdot-}$ complex that is 2.3 kcal/mol lower in energy compared to the RC. A representative structure of the PD with a Fe-O distance of 3.1 Å shows that the dioxygen is bound in an end-on fashion to the Fe-center at a position *trans* to H189 (Figure 4E). In agreement with these results, the elongated Fe-O distance in the Fe(III)-$OO^{\cdot-}$ complex in the septet spin state was observed in previous QM/MM calculations of EFE.[11] The 2OG maintains an *off-line* binding mode with a N_{H189}-Fe-O2-O1 dihedral angle of 107° in the PD.

Thus, by contrast with the results for PHF8, the formation of an off-line Fe(III)-$OO^{-\cdot}$ in EFE is more energetically favorable. The generation of an in-line Fe(III)-$OO^{-\cdot}$ intermediate in EFE is predicted to be energetically unfeasible because the 2OG rearranges to an unusual monodentate coordination mode. In EFE, the substrate is not involved in the dioxygen diffusion tunnel or the stabilization of a Fe(III)-$OO^{-\cdot}$ intermediate, whereas in PHF8, the substrate makes up part of tunnel-1 and is involved in the stabilization of the in-line Fe(III)-$OO^{-\cdot}$ intermediate.

Conclusions

The current study informs on the hypothesis that the local interactions in the non-heme Fe(II)-centers of PHF8 and FFE control the differences in dioxygen and 2OG binding modes to generate *off-line* or *in-line* Fe(III)-$OO^{-\cdot}$ intermediates. We explored the dioxygen diffusion channels in PHF8 and EFE and showed that in both enzymes, the dioxygen could approach the non-heme Fe(II)-centers with binding that leads to the generation of *in-line* or *off-line* Fe(III)-$OO^{-\cdot}$ intermediates. Notably, the QM/MM MetD study on PHF8 indicated that the formation of an *in-line* Fe(III)-OO^{-} intermediate is energetically favorable in contrast to the formation of an *off-line* Fe(III)-$OO^{-\cdot}$ intermediate. The *in-line* dioxygen binding to the Fe(II)-center in PHF8 is stabilized by favorable interactions with residues in

the histone K9me2 substrate along with I191 and T244. These results indicate flexibility in the 2OG binding mode to generate an *in-line* Fe(III)-$OO^{-\cdot}$ intermediate in PHF8 is in agreement with earlier QM/MM calculations that indicated the *in-line* Fe(III)-$OO^{-\cdot}$ intermediate can undergo activation without 2OG rearrangement to generate Fe(IV)=O, which in turn can efficiently perform hydroxylation of the substrate.[19] By contrast, the QM/MM MetD analysis of dioxygen binding to EFE suggests the formation of an *off-line* Fe(III)-$OO^{-\cdot}$ intermediate is energetically preferred. Interactions with A198, F250, A281, and F283 stabilize the *off-line* dioxygen binding to Fe(II) in EFE. These EFE results confirm the 2OG binding mode observed in EFE crystal structures[8–10] and the QM/MM calculations that only an *off-line* Fe(III)-$OO^{-\cdot}$ intermediate can generate ethylene.[12] Overall, the study demonstrates that the protein environment plays a vital role in dioxygen transport and the SCS interactions control the binding mode of the dioxygen in the iron center in PHF8 and EFE.

Experimental Section

System setup and MD simulation:

A crystal structure (PDB ID:3KV4) of PHF8 complexed with $H3_{1-14}$K4me3.K9me2 (corresponding to the first 14 residues of histone H3 with trimethylated Lys4 and dimethylated Lys9) as the peptide fragment of the substrate and N-oxalylglycine (NOG, a 2OG analog) was used for initial modeling.[35] For EFE, the crystal structure (PDB ID:5V2Y) with EFE bound to the Fe analog Mn, the co-substrate 2OG, and the substrate L-Arg was used.[9] Metal Center Parameter Builder (MCPB.py) was used to generate non-heme Fe center parameters.[21,37] MD simulations were performed using Amber16.[38] Details for the system setup and MD simulations are provided in the SI (Pages 1 and 2).

Dioxygen Diffusion Dynamics

The dioxygen diffusion pathways in the PHF8 and EFE ES complexes were explored by running 1 μs MD simulations in the presence of dioxygen molecules. 100 dioxygen molecules were added in the simulation box volume of 685,584 $Å^3$. In agreement with other computational studies on dioxygen diffusion,[26,27] a much greater concentration of the dioxygen molecules was used in the simulation compared to the dioxygen concentration in ambient conditions to maximize chances of dioxygen diffusion and increase sampling of the diffusion channels. The 100 dioxygen molecules were randomly distributed outside the protein using PACKMOL software.[39] The MD simulations were carried out using the same protocol as described in SI. Potential dioxygen transport channels were manually inspected from the MD simulations and characterized with CAVER 3.0.[33]

QM/MM MD and Metadynamics Simulations

The final equilibrated structures from the classical MD simulations were used as initial structures for QM/MM MD simulations of the PHF8 and EFE ES complexes. The QM/MM Born-Oppenheimer MD simulations were performed with CP2K version 6.1, combining QUICKSTEPS for the QM part and FIST for the MM part.[40,41] The QM region consisted of the non-heme Fe, directly coordinating residues, and the substrate (PHF8: K9me2; EFE: L-Arg). The QM region was treated at UB3LYP with D3 dispersion correction, employing

the dual basis set of Gaussian and plane-waves (GPW) formalism.[41] The Gaussian double-ζ valence polarized (DZVP) basis set was used to expand the wave function.[42] The auxiliary plane-waves basis set was expanded using a cutoff of 360 Ry and GTH pseudopotentials.[43] A hydrogen atom was used to cap bonds at the QM-MM boundary. The remaining parts of the systems other than the QM regions were treated at the MM level with parameters developed for the classical MD simulations. The auxiliary density matrix method (ADMM) was used to speed up the Hartree-Fock exchange calculations within UB3LYP.[44] All the QM/MM MD simulations were performed in an NVT ensemble with a time step of 0.5 fs. The PHF8 and EFE ES QM/MM MD simulations were each performed for a total time of 10 ps.

The well-tempered QM/MM Metadynamics method explored the free energy of dioxygen binding to the non-heme Fe(II)-centers in PHF8 and EFE.[45] The distance between the dioxygen and Fe was used as a collective variable (CV). A Gaussian height of 0.6 kcal/mol and width of 0.3 kcal/mol was used for the calculations. The time interval between Gaussian height deposition was kept at 10 fs. The simulations were run until several recrossing between the reactant and product were observed.

Supplementary Material

Refer to Web version on PubMed Central for supplementary material.

Acknowledgment

This research was supported by NIH grant 1R15GM139118 to C.Z.C. and C.J.S. and NSF grants 2203630 to C.Z.C., and 2203472 to J.H. and R.P.H. In addition, S.S.C. would like to acknowledge a doctoral finishing fellowship from the Graduate School and a Health Research Institute fellowship at Michigan Technological University.

References

[1]. Schofield CJ, Hausinger R, 2-Oxoglutarate-Dependent Oxygenases (Eds.: Schofield CJ, Hausinger R), Metallobiology; Royal Society Of Chemistry, Cambridge, 2015, pp. 1–58.

[2]. Herr CQ, Hausinger RP, Trends Biochem. Sci. 2018, 43, 517–532. [PubMed: 29709390]

[3]. Martinez S, Hausinger RP, J. Biol. Chem. 2015, 290, 20702–20711. [PubMed: 26152721]

[4]. Solomon EI, Goudarzi S, Sutherlin KD, Biochemistry 2016, 55, 6363–6374. [PubMed: 27792301]

[5]. Solomon EI, Light KM, L. L. V., Srnec M, Wong SD, Acc. Chem. Res. 2013, 46, 2725–2739. [PubMed: 24070107]

[6]. Costas M, Mehn MP, Jensen MP, Que L, Chem. Rev. 2004, 104, 939–986. [PubMed: 14871146]

[7]. Clifton IJ, McDonough MA, Ehrismann D, Kershaw NJ, Granatino N, Schofield CJ, J. Inorg. Biochem. 2006, 100, 644–669. [PubMed: 16513174]

[8]. Copeland RA, Davis KM, Shoda TKC, Blaesi EJ, Boal AK, Krebs C, Bollinger JM, J. Am. Chem. Soc. 2021, 143, 2293–2303. [PubMed: 33522811]

[9]. Martinez S, Fellner M, Herr CQ, Ritchie A, Hu J, Hausinger RP, J. Am. Chem. Soc. 2017, 139, 11980–11988. [PubMed: 28780854]

[10]. Zhang Z, Smart TJ, Choi H, Hardy F, Lohans CT, Abboud MI, Richardson MSW, Paton RS, McDonough MA, Schofield CJ, Proc. Natl. Acad. Sci. 2017, 114, 4667–4672. [PubMed: 28420789]

[11]. Xue J, Lu J, Lai W, Phys. Chem. Chem. Phys. 2019, 21, 9957–9968. [PubMed: 31041955]

[12]. Chaturvedi SS, Ramanan R, Hu J, Hausinger RP, Christov CZ, ACS Catal. 2021, 11, 1578–1592.

[13]. Yeh C-CG, Ghafoor S, Satpathy JK, Mokkawes T, Sastri CV, de Visser SP, ACS Catal. 2022, 12, 3923–3937.

[14]. Hausinger RP, Crit. Rev. Biochem. Mol. Biol. 2004, 39, 21–68. [PubMed: 15121720]

[15]. Elkins JM, Ryle MJ, Clifton IJ, Dunning Hotopp JC, Lloyd JS, Burzlaff NI, Baldwin JE, Hausinger RP, Roach PL, Biochemistry 2002, 41, 5185–5192. [PubMed: 11955067]

[16]. Dann CE, Bruick RK, Deisenhofer J, Proc. Natl. Acad. Sci. 2002, 99, 15351–15356. [PubMed: 12432100]

[17]. Yu B, Edstrom WC, Benach J, Hamuro Y, Weber PC, Gibney BR, Hunt JF, Nature 2006, 439, 879–884. [PubMed: 16482161]

[18]. Zhang Z, Ren J, Harlos K, McKinnon CH, Clifton IJ, Schofield CJ, FEBS Lett. 2002, 517, 7–12. [PubMed: 12062399]

[19]. Chaturvedi SS, Ramanan R, Lehnert N, Schofield CJ, Karabencheva-Christova TG, Christov CZ, ACS Catal. 2020, 10, 1195–1209. [PubMed: 31976154]

[20]. Copeland RA, Zhou S, Schaperdoth I, Shoda TKC, Bollinger JM, Krebs C, Science 2021, 373, 1489–1493. [PubMed: 34385355]

[21]. Waheed SO, Ramanan R, Chaturvedi SS, Lehnert N, Schofield CJ, Christov CZ, Karabencheva-Christova TG, ACS Cent. Sci. 2020, 6, 795–814. [PubMed: 32490196]

[22]. Chaturvedi SS, Ramanan R, Waheed SO, Karabencheva-Christova TG, Christov CZ, in Adv. Protein Chem. Struct. Biol 2019, pp. 113–125. [PubMed: 31564306]

[23]. Wang B, Usharani D, Li C, Shaik S, J. Am. Chem. Soc. 2014, 136, 13895–13901. [PubMed: 25203306]

[24]. Wang B, Cao Z, Sharon DA, Shaik S, ACS Catal. 2015, 5, 7077–7090.

[25]. Visser SP, Chem. Eur. J. 2020, 26, 5308–5327. [PubMed: 31804749]

[26]. Torabifard H, Cisneros GA, Chem. Sci. 2017, 8, 6230–6238. [PubMed: 28989656]

[27]. Domene C, Jorgensen C, Schofield CJ, J. Am. Chem. Soc. 2020, 142, 2253–2263. [PubMed: 31939292]

[28]. Fontecilla-Camps JC, Volbeda A, Chem. Rev. 2022, 122, 12110–12131. [PubMed: 35536891]

[29]. Bhunia S, Ghatak A, Dey A, Chem. Rev. 2022, 122, 12370–12426. [PubMed: 35404575]

[30]. Chaturvedi SS, Jaber Sathik Rifayee SB, Waheed SO, Wildey J, Warner C, Schofield CJ, Karabencheva-Christova TG, Christov CZ, JACS Au 2022, 2, 2169–2186. [PubMed: 36186565]

[31]. Gora A, Brezovsky J, Damborsky J, Chem. Rev. 2013, 113, 5871–5923. [PubMed: 23617803]

[32]. Kohen A, Acc. Chem. Res. 2015, 48, 466–473. [PubMed: 25539442]

[33]. Chovancova E, Pavelka A, Benes P, Strnad O, Brezovsky J, Kozlikova B, Gora A, Sustr V, Klvana M, Medek P, Biedermannova L, Sochor J, Damborsky J, PLoS Comput. Biol. 2012, 8, e1002708. [PubMed: 23093919]

[34]. Chaturvedi SS, Ramanan R, Waheed SO, Ainsley J, Evison M, Ames JM, Schofield CJ, Karabencheva-Christova TG, Christov CZ, Chem. Eur. J. 2019, 25, 5422–5426. [PubMed: 30817054]

[35]. Horton JR, Upadhyay AK, Qi HH, Zhang X, Shi Y, Cheng X, Nat. Struct. Mol. Biol. 2010, 17, 38–43. [PubMed: 20023638]

[36]. Yu L, Wang Y, Huang S, Wang J, Deng Z, Zhang Q, Wu W, Zhang X, Liu Z, Gong W, Chen Z, Cell Res. 2010, 20, 166–173. [PubMed: 20101266]

[37]. Li P, Merz KM, J. Chem. Inf. Model. 2016, 56, 599–604. [PubMed: 26913476]

[38]. Case DA, Belfon K, Ben-Shalom IY, Brozell SR, Cerutti DS, T. E. C. III, Cruzeiro VWD, Darden TA, Duke RE, Giambasu G, Gilson MK, Gohlke H, Goetz AW, Harris R, Izadi S, Kazavajhala K, Kovalenko A, Krasny R, Kurtzman T, Lee TS, LeGrand S, Li P, Lin C, Liu J, Luchko T, Luo R, Man V, Merz KM, Miao Y, Mikhailovskii O, Monard G, Nguyen H, Onufriev A, Pantano S, Pan F, Qi R, Roe DR, Roitberg A, Sagui C, Schott-Verdugo S, Shen J, Simmerling CL, Skynnikov N, Smith J, Swails J, Walker RC, Wang J, Wilson L, Wolf V, Wu X, York DM, Kollman PA, AMBER 2016, University of California, San Francisco, 2016.

[39]. Martínez L, Andrade R, Birgin EG, Martínez JM, J. Comput. Chem. 2009, 30, 2157–2164. [PubMed: 19229944]

[40]. Kühne TD, Iannuzzi M, Del Ben M, Rybkin VV, Seewald P, Stein F, Laino T, Khaliullin RZ, Schütt O, Schiffmann F, Golze D, Wilhelm J, Chulkov S, Bani-Hashemian MH, Weber V, Borštnik U, Taillefumier M, Jakobovits AS, Lazzaro A, Pabst H, Müller T, Schade R, Guidon M, Andermatt S, Holmberg N, Schenter GK, Hehn A, Bussy A, Belleflamme F, Tabacchi G, Glöß A, Lass M, Bethune I, Mundy CJ, Plessl C, Watkins M, VandeVondele J, Krack M, Hutter J, J. Chem. Phys. 2020, 152, 194103. [PubMed: 33687235]

[41]. VandeVondele J, Krack M, Mohamed F, Parrinello M, Chassaing T, Hutter JQ, Comput. Phys. Commun. 2005, 167, 103–128.

[42]. VandeVondele J, Hutter J, J. Chem. Phys. 2007, 127, 114105. [PubMed: 17887826]

[43]. Goedecker S, Teter M, Hutter J, Phys. Rev. B 1996, 54, 1703–1710.

[44]. Guidon M, Hutter J, VandeVondele J, J. Chem. Theory Comput 2010, 6, 2348–2364. [PubMed: 26613491]

[45]. Barducci A, Bussi G, Parrinello M, Phys. Rev. Lett. 2008, 100, 020603. [PubMed: 18232845]

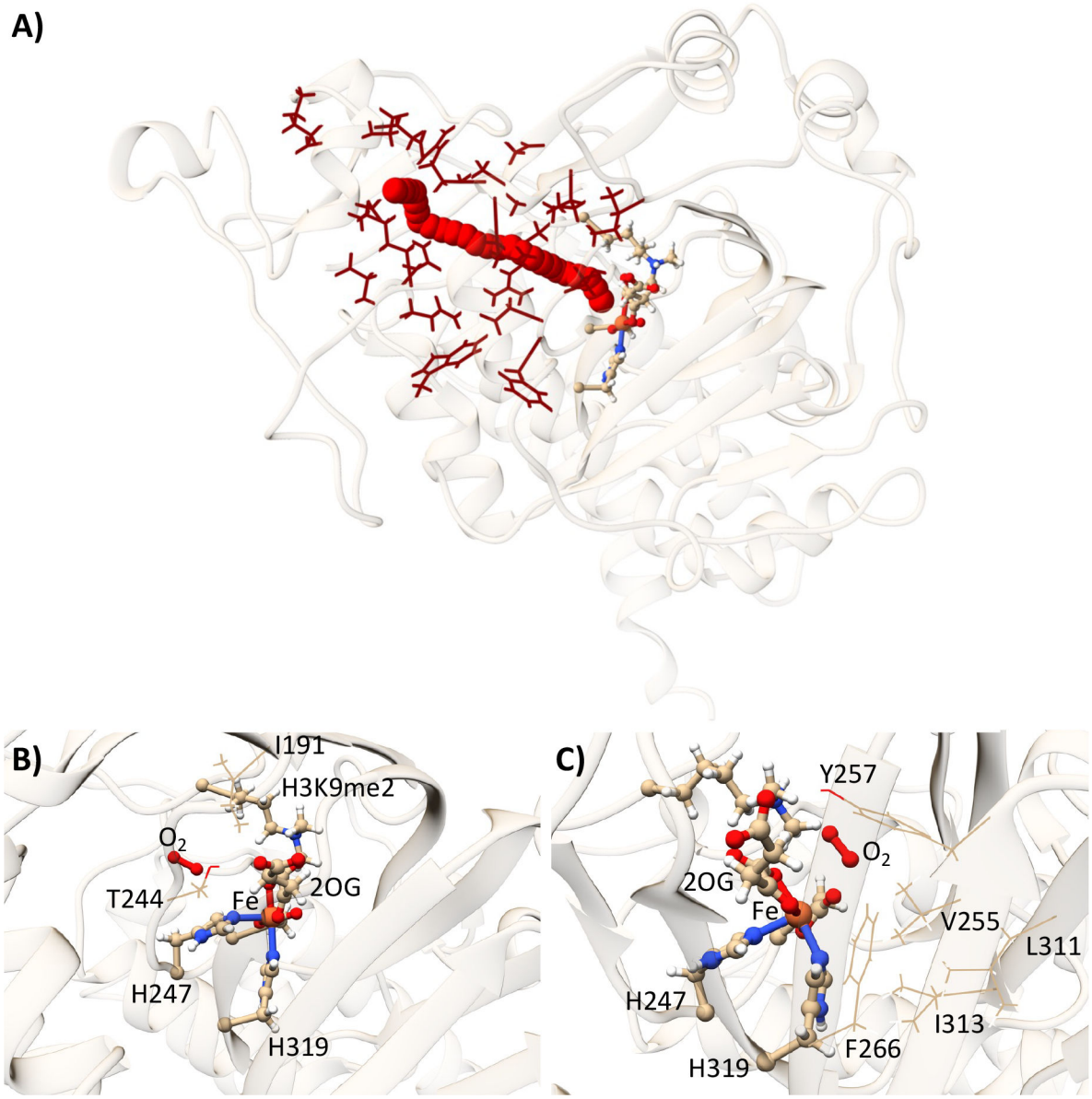

Figure 1.

Dioxygen (O_2) transport in PHF8. (A) Dioxygen (O_2) transport in PHF8 via tunnel-1 obtained from diffusion dynamics. The tunnel residues are not labeled here for clarity but are shown in detail in Figures S5–S7. (B) The approach of dioxygen to the Fe(II)-center for likely formation of an *in-line* Fe(III)-$OO^{-\cdot}$ complex following 2OG rearrangement. (C) The dioxygen approach for likely formation of an *off-line* Fe(III)-$OO^{-\cdot}$ complex. The Fe(II)-center, dioxygen, 2OG, and H3K9me2 substrates are shown as balls and sticks.

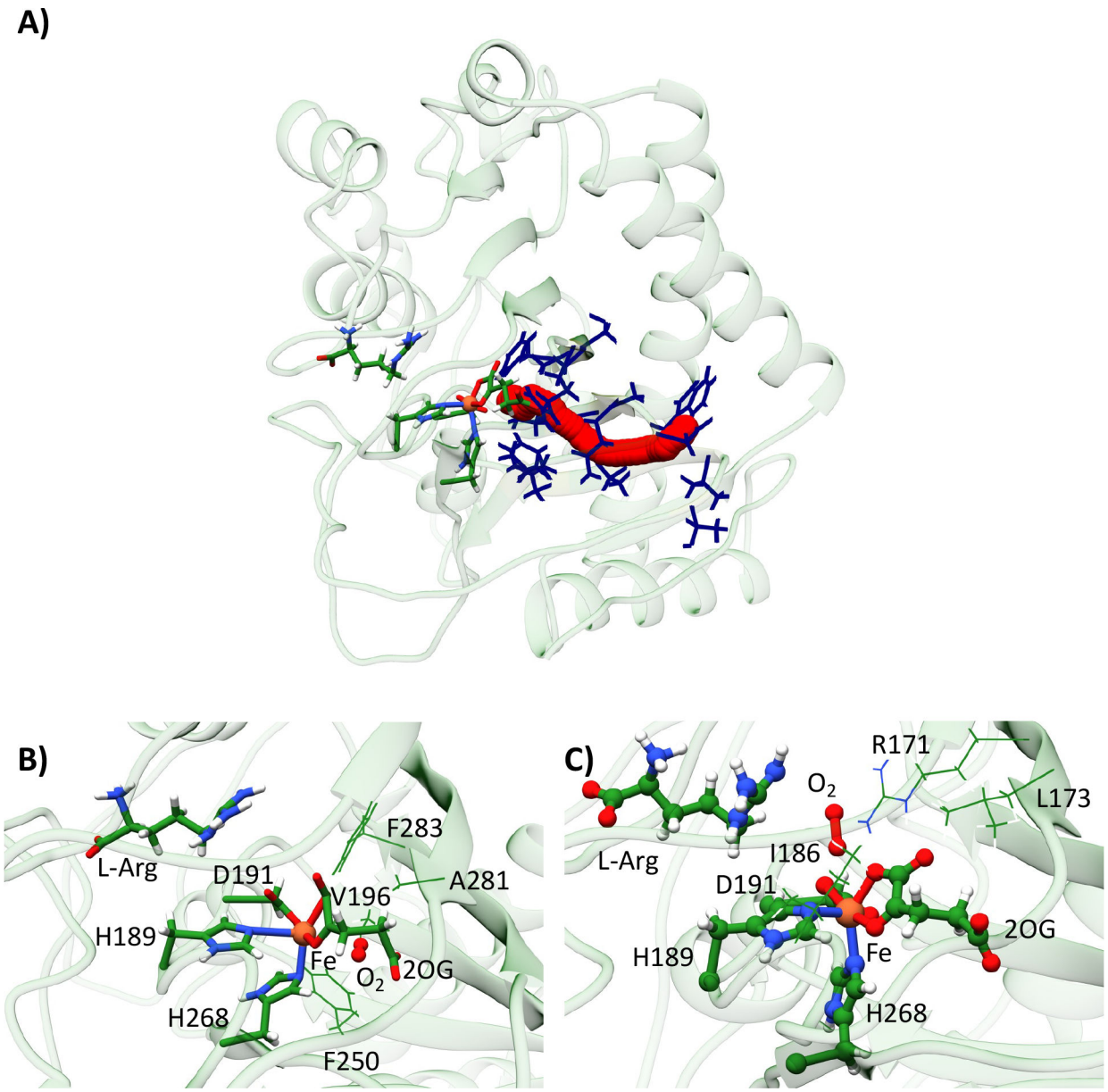

Figure 2. Dioxygen (O_2) transport in EFE.

(A) Dioxygen (O_2) transport in EFE via tunnel-1 obtained from diffusion dynamics; the tunnel residues are not labeled here for clarity and are shown in detail in Figures S10–S12. (B) The *off-line* dioxygen approach through tunnel-1 in EFE for binding to the Fe(II)-center forms an *off-line* Fe(III)-$OO^{-\cdot}$ complex. (C) The *in-line* approach of dioxygen through tunnel-2 for binding to the Fe(II)-center in EFE, leading to formation of an *in-line* Fe(III)-$OO^{-\cdot}$ complex with 2OG rearrangement. The Fe(II)-center, dioxygen, 2OG, and H3K9me2 substrate are shown as balls and sticks.

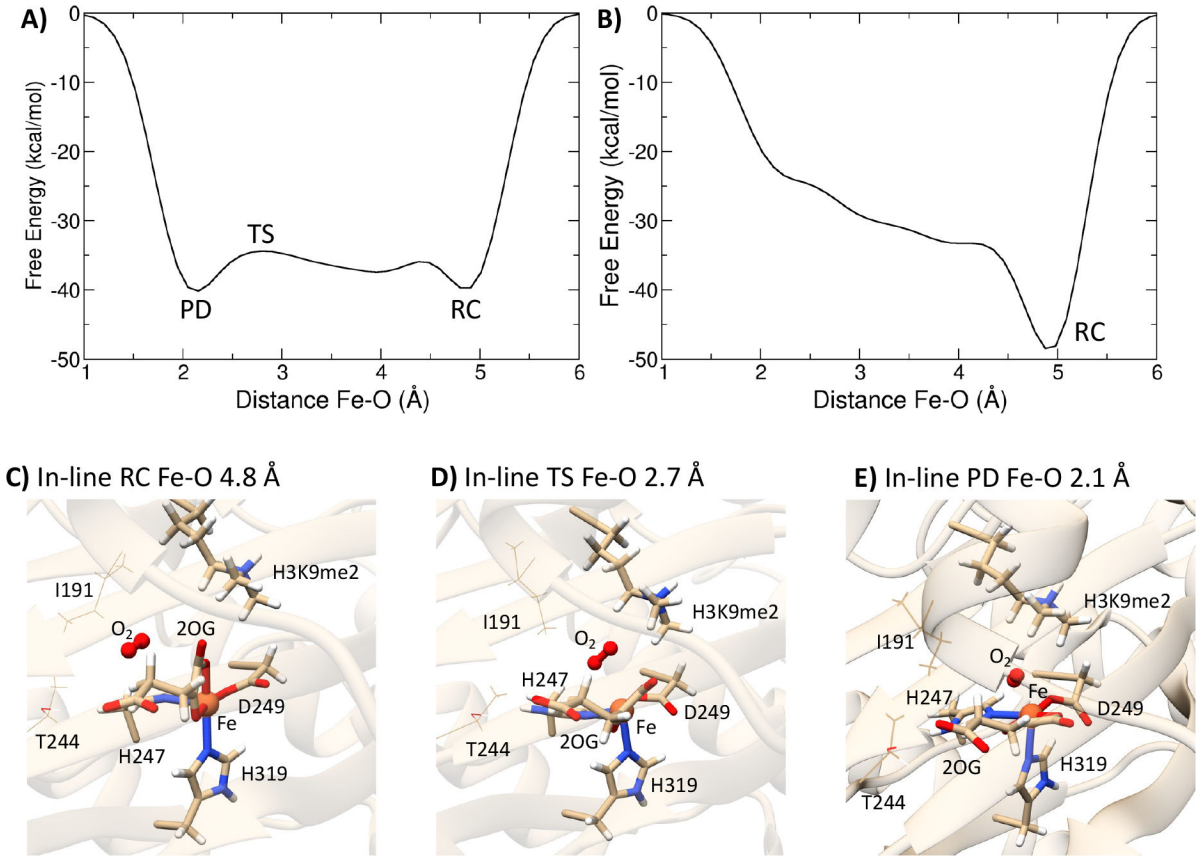

Figure 3. QM/MM MetD free energy surfaces for dioxygen binding in PHF8.

Free energy versus Fe-O distance plots are shown for generation of (A) the *in-line* Fe(III)-$OO^{\cdot-}$ complex and (B) the *off-line* Fe(III)-$OO^{\cdot-}$ complex. Representative structures for (C) *in-line* dioxygen binding RC, (D) *in-line* dioxygen binding TS, and (E) *in-line* dioxygen binding PD are obtained from QM/MM MetDs.

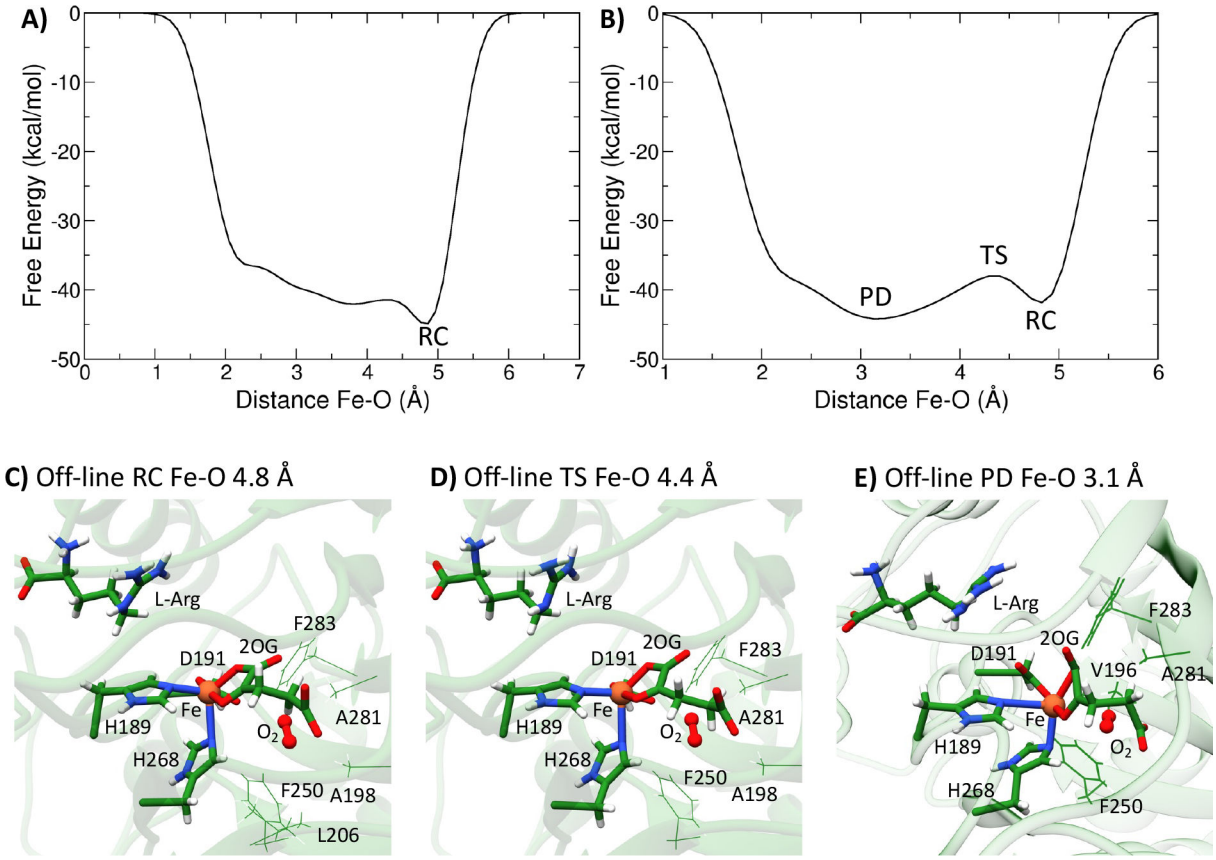

Figure 4. Free energy surfaces for dioxygen binding in EFE.

Free energy versus Fe-O distance plots for generation of (A) an *in-line* Fe(III)-$OO^{\cdot-}$ complex and (B) an *off-line* Fe(III)-$OO^{\cdot-}$ complex. Representative structures for (C) *off-line* dioxygen binding RC, (D) *off-line* dioxygen binding TS, and (E) *off-line* dioxygen binding PD were obtained from QM/MM MetD.